OPEN ACCESS
IOP Publishing
Plasma Sources Science and Technology
Plasma Sources Sci. Technol. **26** (2017) 025007 (10pp)
doi:10.1088/1361-6595/26/2/025007

On the E-H transition in inductively coupled radio frequency oxygen plasmas: II. Electronegativity and the impact on particle kinetics

Th Wegner[1], **C Küllig and J Meichsner**

Institute of Physics, University of Greifswald, Felix-Hausdorff-Str. 6, 17489 Greifswald, Germany

E-mail: physics@thwegner.com and meichsner@physik.uni-greifswald.de

Received 29 July 2016, revised 9 October 2016
Accepted for publication 18 November 2016
Published 19 January 2017

Abstract

In this series of two papers we present results about the E-H transition of an inductively coupled oxygen discharge driven at radio frequency (13.56 MHz) for different total gas pressures. The mode transition from the low density E-mode to the high density H-mode is studied using comprehensive plasma diagnostics. The measured electron density can be used to distinguish between the different operation modes. This paper focuses on the determination of the negative atomic ion density and the electronegativity by two experimental methods and global rate equation calculation. As a result, the electronegativity significantly decreases over two orders of magnitude from about 25 in the E-mode to about 0.1 in the H-mode. The temporal behavior of the electronegativity in pulsed ICP shows that the negative atomic ion density reaches a steady state after 10 ms. Negative atomic ions are mainly produced by the dissociative attachment with the molecular ground state. The ion–ion recombination with the positive molecular ions and the collisional detachment with the singlet molecular metastables contribute significantly to the loss of the negative atomic ions.

Keywords: inductively coupled plasma, oxygen, mode transition, microwave interferometry, laser photodetachment, electronegativity

(Some figures may appear in colour only in the online journal)

1. Introduction

Inductively coupled plasmas (ICP) which are driven at radio frequency (RF) have unique properties and have been applied in plasma processing for decades [1]. Oxygen ICP, especially, are often used for plasma surface treatments [2–9]. The presence of negative ions influences the plasma properties, such as the charged species balance, plasma chemical reactions, diffusion of charged particles and the electron energy distribution function. Furthermore, they can induce plasma instabilities which are well known in the literature [10–13]. Hence, knowledge about the fraction of negative ions is important in characterizing the discharge. In particular, the change of the negative ion density and the electronegativity, defined as the ratio between negative ion and electron density, has been sparsely studied during the E-H transition.

The ICP operates in the E-mode at low RF power with low plasma density and high sheath voltage. At a critical electron density, the mode transition takes place. The observed mode transition can be continuous or steplike. The continuous transition, observed at lower total gas pressure, is connected

[1] Present address: Max-Planck-Institute for Plasma Physics, Wendelsteinstr. 1, 17491 Greifswald, Germany

with the appearance of the E- and H-mode simultaneously. That means the ICP operates in a hybrid mode. With further increase of the RF power, the discharge transits in the H-mode with high plasma density and low sheath voltage. During the mode transition, the electron heating mechanisms, the determining elementary processes, e.g. production and loss of negative atomic ions, and the plasma parameters change significantly.

Stoffels *et al* [14] studied the negative ion dynamics in a capacitively coupled plasma (CCP) in oxygen. They showed that O^- is the dominant negative ion, whereas the O_2^- and O_3^- reach about 10% of the total negative ion density. They furthermore reported that the electronegativity varies between 5 and 10 and changes with pressure and RF power. Katsch *et al* studied a CCP [15] and ICP [16] in oxygen. With increasing RF power, they determined a decreasing electronegativity for the CCP. Additionally, the electronegativity in their ICP was higher compared to their CCP. Gudmundsson *et al* [17] used a global model to investigate the negative ions and metastable species in a low pressure, high density oxygen plasma. They also found that O^- is the dominant negative ion and reported on the main elementary processes. Corr *et al* [18] studied the plasma parameters of an oxygen ICP, e.g. electron and negative atomic ion density, atomic ground state density, for different RF power and total gas pressure. They used Langmuir probe diagnostics, laser photodetachment and two-photon laser-induced fluorescence. Furthermore, they supplemented their measurements with a global model. The authors showed that the electronegativity in the E-mode is about 10 and hence two orders of magnitude higher compared to the H-mode. They explained the decreasing electronegativity during the E-H transition by the increasing dissociation of the molecular ground state, which is important for the production of negative ions. Many works have reported that the main mechanism for the production of the negative atomic ions is the attachment with the molecular ground state [14, 17], whereas the loss processes are mainly due to ion–ion recombination at low total gas pressure and detachment with the atomic ground state and the singlet molecular metastable state at higher pressure [14], [16–19]. Toneli *et al* [20] described a global model for an oxygen ICP and considered an extensive reaction equation set. They figured out, to the contrary, that the lower singlet molecular metastable state has only a small influence on the loss of negative atomic ions. At low total gas pressure ($<$0.3 Pa), the electron impact detachment is very effective, while the detachment by the atomic ground state and the higher singlet molecular metastable state become the most effective loss process up to 7 Pa. They furthermore showed that the charge exchange is the most important loss process of the negative atomic ion for total gas pressures above 7 Pa. Nevertheless, the behavior of the negative ions as well as the electronegativity during the mode transition of a pure oxygen ICP is not studied in these works.

In this second paper of the two paper series we report on experimental results about the E-H transition which are supplemented by a global rate equation calculation. We apply comprehensive plasma diagnostics to investigate the plasma parameters during the E-H transition with high RF power resolution. In this contribution, we present the negative atomic ion density as well as the electron density to calculate the electronegativity. The experimental results are compared with a global rate equation calculation, which enables an estimation for the most important elementary processes for the production and loss of the negative atomic ions. The results presented in this paper together with that given in Wegner *et al* [21] provide an extensive set of input parameters for modeling/simulation of oxygen ICP and extend the knowledge about the E-H transition.

The paper firstly describes the experimental setup and the used diagnostics. In particular, it explains the microwave interferometry and the laser photodetachment. In this section, a two dimensional calculation of the detachment signal is given and reveals an optimal setup of the laser arrangement. Secondly, the negative atomic ion density as well as the electronegativity were experimentally determined via an electron density peak in the early afterglow and laser photodetachment. Furthermore, the temporally resolved electronegativity was determined in the plasma phase of a pulsed ICP. The experimental results are supplemented by a global rate equation calculation, which gives information about important elementary processes. All methods reveal comparable results and show that the electronegativity strongly decreases during the E-H transition.

2. Experimental setup and diagnostics

2.1. Vacuum chamber and discharge arrangement

The experimental setup involves a vacuum chamber, discharge arrangement and plasma diagnostics, see figure 1. The vacuum chamber and ICP configuration are as previously described by Wegner *et al* [22]. The cylindrical vacuum chamber (400 mm in diameter) is grounded and equipped with vacuum pumps and control units. A base pressure less than 10^{-5} Pa and a total gas pressure for plasma processing between 1 and 15 Pa were set by a turbomolecular pump and a rotary vane pump respectively. Oxygen was used as processing gas, and was injected at a constant gas flow rate of 5 sccm. The inductive discharge arrangement is immersed in the plasma from above and is composed of a planar coil installed inside a quartz cylinder. The quartz cylinder acts as dielectric barrier and separates the coil from the vacuum. The center connection of the coil ($r = 0$) is powered while the two opposite ends of the coil are on ground potential. The output of the RF power generator was varied between 1 and 600 W, yielding to a (peak-to-peak) coil voltage between 1 and 9 kV and a (peak-to-peak) coil current between 1 and 50 A. The RF power resolution was minimal 1 W for low RF power values and in the region of the E-H transition. Furthermore, the matching network was fixed to minimize its influence on the discharge. The resulting reflected RF power was smaller than 5% of the input power. The discharge was pulsed with a frequency of 10 Hz and a duty cycle of 50%. Therefore, the plasma was ON and OFF for 50 ms each. The generated plasma was axially

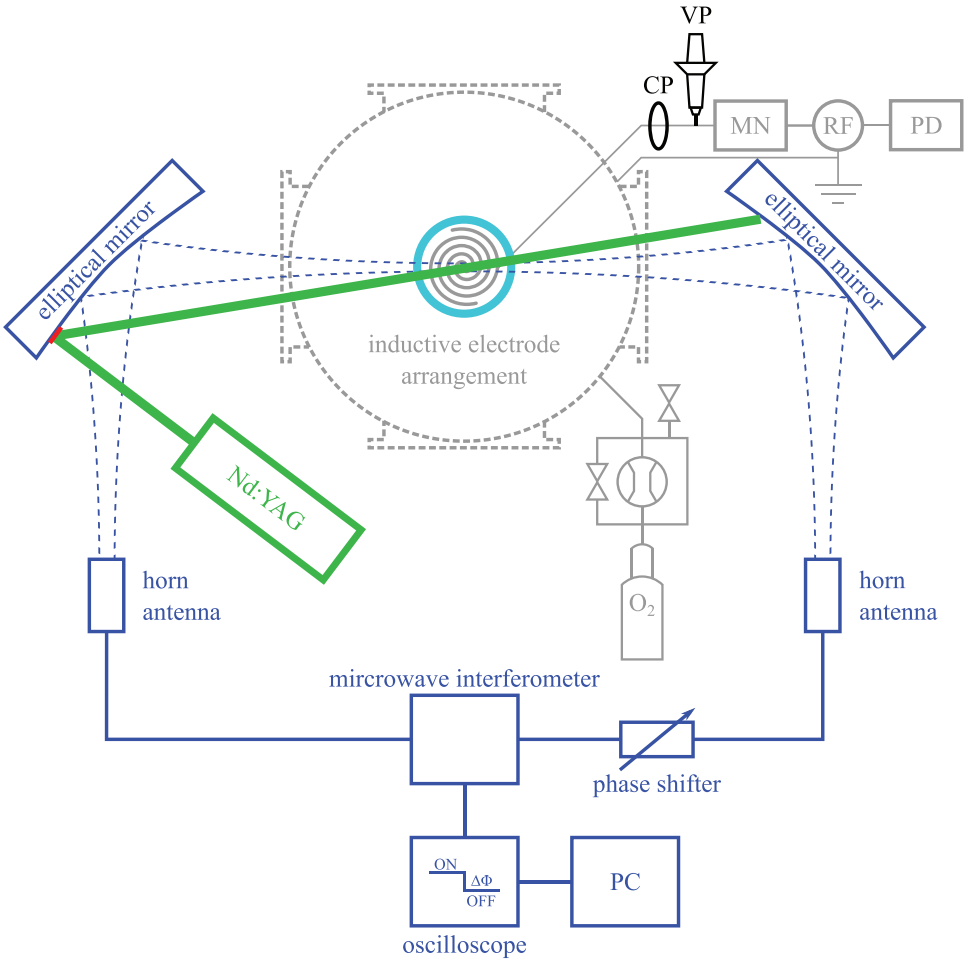

Figure 1. Schematic top view of the discharge vessel with the gas supply, matching network (MN), power supply (RF) and the pulse delay generator (PD). The used diagnostics are the current (CP) and voltage probes (VP), the 160 GHz microwave interferometer and a Nd:YAG laser respectively.

confined between the bottom of the quartz cylinder (120 mm in diameter) at $a = 0$ and the top of a grounded stainless steel electrode (100 mm in diameter) at $a = 50$ mm.

2.2. Plasma diagnostics

The electronegativity of the oxygen ICP was determined by Gaussian beam microwave interferometry, measuring the bulk plasma electron density and the density of the temporally released electrons after the laser pulse. The applied 160 GHz microwave interferometry was as previously described by Dittmann *et al* [23]. It reveals information about the line integrated electron density by measuring the phase shift $\Delta\Phi$ between the plasma ON and OFF phase using

$$\Delta\Phi = \frac{\pi}{n_C\ \lambda_{MWI}} \int n_e(r)\ \mathrm{d}r = \frac{\pi}{n_C\ \lambda_{MWI}}\ \tilde{n}_e, \qquad (1)$$

where $n_e(r)$, n_C and λ_{MWI} are the the radial distribution of the electron density, the critical electron density and the microwave wavelength respectively. The temporal resolution is about 200 ns, being limited by filters and video-amplifier. The line integrated electron density resolution is about $5.3 \times 10^{13}\ \mathrm{m}^{-2}$.

The negative atomic ion O^- has an electron affinity of 1.46 eV [24], which defines the minimum photon energy necessary for the release of an electron from the negative atomic ion

$$O^- + h\nu \longrightarrow e + O,$$

where h and ν are the Planck constant and the laser frequency respectively. Therefore, the second harmonic of a neodymium-doped yttrium–aluminum garnet (Nd:YAG) laser was used at the wavelength of 532 nm. The corresponding photon energy of about 2.3 eV is sufficiently high for the detachment of all negative ions. Nevertheless, previous works have shown that the negative molecular ion density is low compared to the negative atomic ion density [14, 15, 24, 25]. The whole laser system is as previously described by Küllig *et al* [26]. Both the repetition frequency of the laser pulse and the discharge pulse frequency amount to 10 Hz. The onset of the laser pulse was set in the temporal middle of the discharge pulse at 25 ms after switching ON the RF power. For another experiment, the onset of the laser shot in relation to the discharge pulse was varied between 0% and 105%. A maximum laser pulse energy of $E_L = 400$ mJ can be achieved at a pulse duration of 7 ns. The laser is axially adjusted in the optical axis of the microwave beam at $a = 30$ mm. The maximum overlapping volume

between the laser and microwave beam has to be realized for an optimal detachment signal. Furthermore, the undisturbed microwave guiding within the aperture limit of the Gaussian beam propagation has to be considered [27]. This limits the position of the laser mirror placed on the elliptical microwave mirror, see figure 1. To ensure a measurable detachment signal with an optimal signal-to-noise ratio, a numerical calculation provides an estimation for an optimal adjustment regarding the laser beam angle φ_L and diameter d_L. Furthermore, the spatial laser beam distribution $l(x, y, \varphi)$ multiplied by the detachment ratio $R(d_L)$ is important for this calculation. The detachment ratio is the fraction between the detached electrons and the negative atomic ion density and is given by [28]

$$R(d_L) = 1 - \exp\left(-\frac{\sigma\, E_L}{h\, \nu\, A(d_L)}\right), \tag{2}$$

where σ and $A = 1/4\ \pi\ d_L^2$ are the photodetachment cross section and the laser beam cross section respectively. The photodetachment cross section $\sigma = 6.35 \times 10^{-22}\ \mathrm{m}^2$ is taken from Burch *et al* [29]. For the detachment signal D estimation, the normalized quantities of the Gaussian microwave beam electric field distribution $E(x, y)$, the detachment ratio $R(d_L)$ multiplied by the laser beam distribution $l(x, y, \varphi)$ resulting to $L(x, y, d_L, \varphi_L)$ and a measured plasma profile $P(x, y)$ were convoluted and integrated over the x-y-plane at $a = 30\,\mathrm{mm}$ for different laser diameters and angles regarding the optical axis of the microwave beam using

$$D(d_L, \varphi_L) = \int\int E(x, y)\, L(x, y, d_L, \varphi_L)\, P(x, y)\, \mathrm{d}x\ \mathrm{d}y. \tag{3}$$

A high overlap volume between the quantities listed above reveals a high detachment signal. The result of this calculation is shown in figure 2. There is a geometrically inaccessible region for an angle between about 12° and 76° due to the position of the vessel ports. Generally, the detachment signal increases with increasing laser diameter up to about 25 mm. Using a laser diameter above 25 mm leads to a lower detachment signal because the energy per area decreases, which finally causes a lower detachment ratio. In this experiment, the laser beam was expanded via lenses to a diameter of 15 mm, giving a detachment ratio of about 96.6% at a laser energy of 350 mJ, which is the lower limit of the laser energy guiding through the plasma. Other measurements show that about 25 mJ is lost due to the reflectivity of the laser mirror and the transmissivity of the laser lenses and discharge vessel windows. Additionally, the laser beam is guided through the plasma with an angle of 8.5° relative to the optical axis of the microwave beam. To enable this laser path, a small laser mirror has to be installed on the microwave mirror, see figure 1. Here, the position of the laser mirror barely fulfills the aperture limit of the Gaussian beam propagation. Furthermore, the comparison of electron density measurements with and without laser mirror shows comparable results.

The measurement procedure was as follows. Both the laser and the discharge were pulsed during all measurements. In particular, the flash lamps and the Pockels cell were pulsed while the shutter of the laser was closed in the first part of each measurement. Nevertheless, the microwave phase shift signal was measured without laser photodetachment. In the second part of each measurement, the shutter was opened and the laser propagated through the plasma, detaching electrons from negative atomic ions. The microwave phase shift signal with a typical peak resulting from the released electrons was recorded. Both signals were averaged over 10 000 pulses and finally subtracted from each other, leading to the pure detachment signal. The height of the detachment peak reveals information about the negative atomic ion density using equation (1).

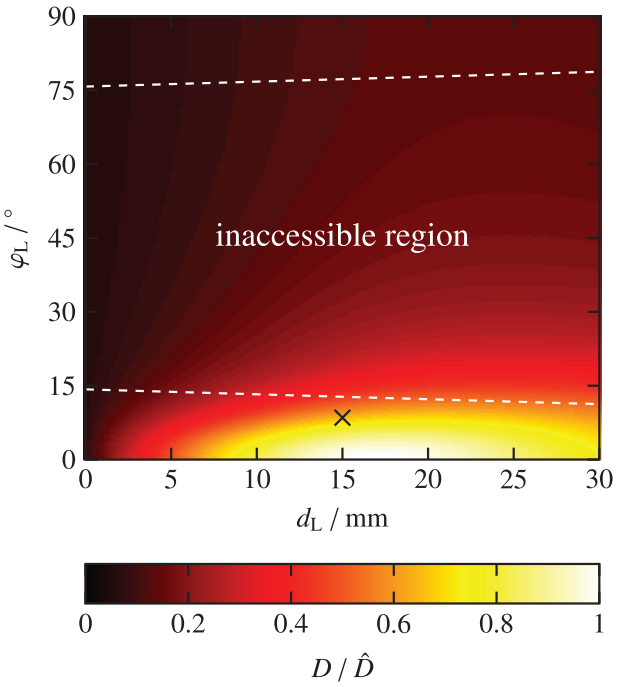

Figure 2. Normalized detachment signal D / $\hat{D}$ taking into account the microwave beam, laser beam and plasma profile for different merging angle φ_L and laser diameter d_L. The white dotted lines indicate the border between the geometrically accessible and inaccessible regions. The cross shows the parameters used for this experiment.

3. Results and discussion

The line integrated electron density was deconvolved to absolute values using profiles measured with the Langmuir probe [21]. Hence, the electron density resolution amounts to about $3 \times 10^{14}\ \mathrm{m}^{-3}$.

A changing electronegativity during the mode transition is reported in previous works. In particular, the study of the electron heating in the E-mode with phase resolved optical emission spectroscopy reveals an electric field reversal [30] during the sheath collapse [31, 32]. This is the result of a drift electric field caused by a depleted conductivity, which can be due to a high electronegativity [25, 33]. The electric field reversal vanishes during the E-H transition and indicates a decreasing electronegativity. Additionally, the determination of the ionization rate also reveals a changing electronegativity [21]. Particularly, the electron density increases during the

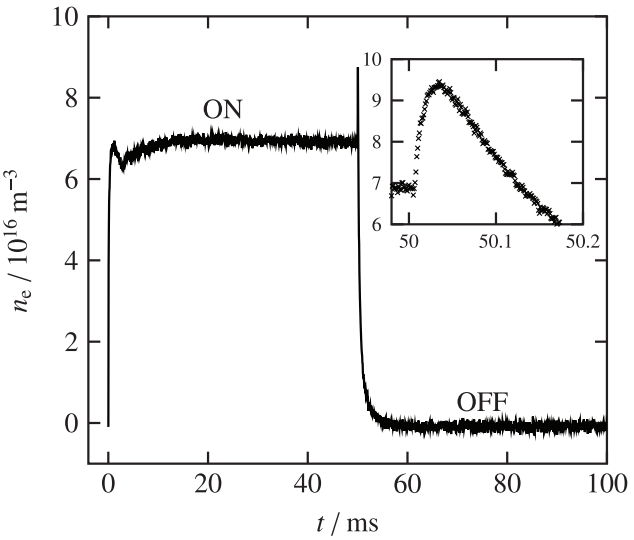

Figure 3. Electron density n_e over time t for a total gas pressure of 5 Pa and RF power of 300 W in the H-mode. The RF power coupling is started at $t = 0$ and disabled at $t = 50$ ms. The subfigure shows a zoom of the electron density peak in the early afterglow.

E-H transition despite the fact that the electron impact ionization rate for molecular ground state oxygen shrinks significantly. This implies that the confinement of electrons due to inductive heating is increased and the loss of electrons due to attachment reactions is reduced, which is combined with decreasing electronegativity. These examples are just qualitative indications for a changing electronegativity. In the following, the electronegativity and the negative atomic ion density were determined using two experimental methods and a rate equation calculation.

3.1. Electron density peak in the early afterglow

The temporally resolved electron density is exemplarily shown in figure 3 for the H-mode at a total gas pressure of 5 Pa. The RF power of 300 W is enabled at $t = 0$ and disabled at $t = 50$ ms. At the beginning of the RF power coupling, the discharge builds up and reaches after about 1 to 5 ms a steady state in which the electron density stays nearly constant. After switching OFF the RF power coupling, the electron density increases quickly and decays over 50 to 300 μs. The further decrease of the electron density after the density peak is due to recombination, diffusion and wall losses. The increase of the electron density in the early afterglow is well known from the literature for CCP [43] and ICP [44] and is mainly the result of the collisional detachment of negative atomic ions by the singlet molecular metastable state $O_2(a^1\Delta_g)$ [43]. This emphasizes the importance of this metastable state. Hence, the height of the electron density peak reveals information about the negative atomic ion density. In the E-mode this additional electron density peak is large compared to the steady state electron density during the discharge pulse. This ratio changes during the E-H transition. In relation to the steady state electron density, the electron density peak is small in the H-mode. As a result, the electron density peak cannot be clearly identified, because its height is comparable to the noise level. The

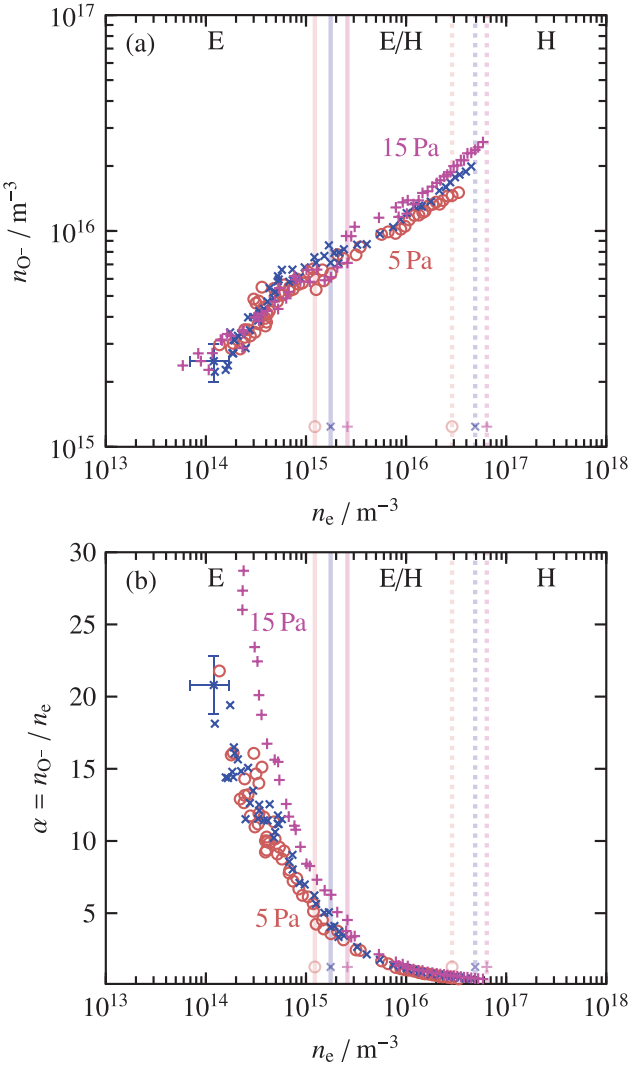

Figure 4. Negative atomic ion density n_{O^-} (a) and electronegativity α (b) determined from the electron density peak in the early afterglow over the electron density n_e for varying total gas pressures (5 Pa (∘), 10 Pa (×) and 15 Pa (+)) for the E-mode (E), the hybrid mode (E/H) and for the H-mode (H). The semi-transparent lines with the associated symbols indicate the electron density at which the E-E/H (solid) and the E/H-H (dotted) transition take place.

negative atomic ion density and the electronegativity determined from the electron density peak in the early afterglow are shown in figures 4(a) and (b) respectively. Generally, the negative atomic ion density increases with raising electron density from about 2×10^{15} to 7×10^{15} m^{-3} in the E-mode to 2×10^{16} m^{-3} in the H-mode. Hence, the electronegativity decreases from about 25 to 4 in the E-mode and to about 0.4 at the E/H-H transition. A clear pressure dependence of both parameters cannot be observed. A prediction about the negative ion density and the electronegativity in the H-mode with this method is not possible.

3.2. Laser photodetachment

Additionally, the negative atomic ion density and the electronegativity were determined via the laser photodetachment. The results are shown in figure 5. Here, the negative atomic

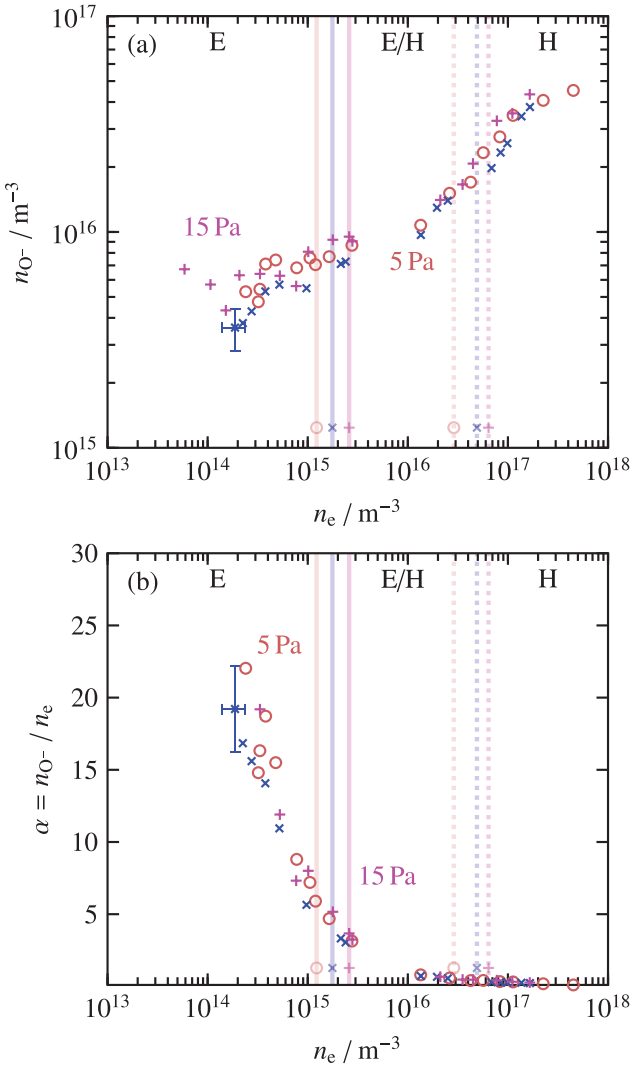

Figure 5. Negative atomic ion density n_{O^-} (a) and electronegativity α (b) determined from the laser photodetachment over the electron density n_e for varying total gas pressures (5 Pa (◦), 10 Pa (×) and 15 Pa (+)) for the E-mode (E), the hybrid mode (E/H) and for the H-mode (H). The semi-transparent lines with the associated symbols indicate the electron density at which the E-E/H (solid) and the E/H-H (dotted) transition take place.

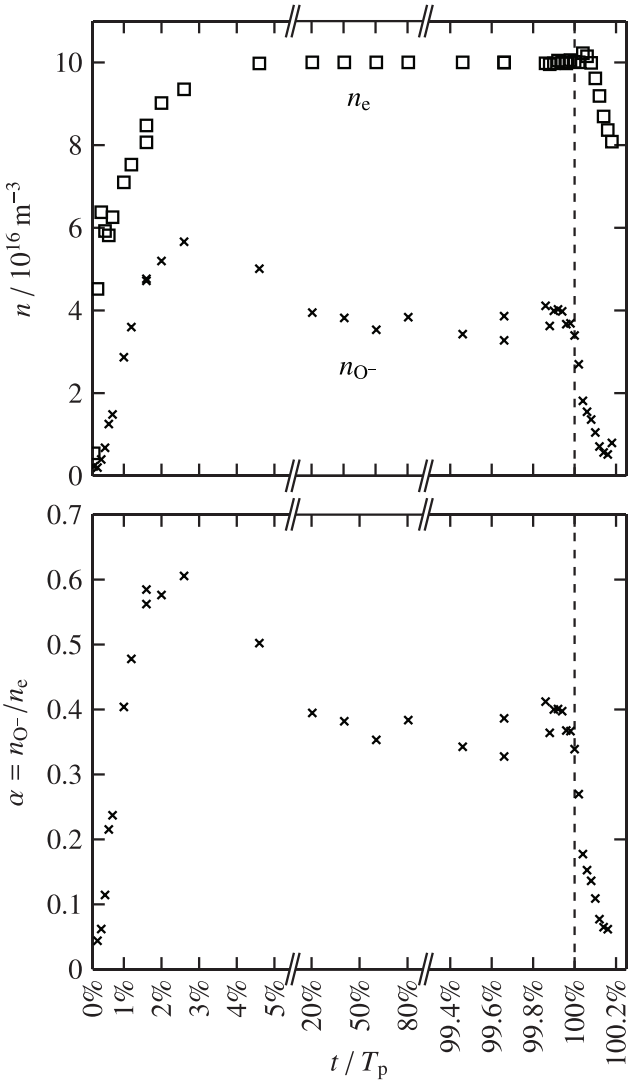

Figure 6. Negative atomic ion density (×) n_{O^-} and electron density (□) n_e (a) and the electronegativity over the onset time of the laser shot in relation to the discharge period time t/T_p for a total gas pressure of 5 Pa for the H-mode (H). The dashed line presents the end of the discharge.

ion density can be measured in the H-mode and reaches a value of about 5×10^{16} m^{-3}. Hence, the electronegativity decreases in the H-mode to about 0.1. Additionally, the time constant for the electron density relaxation after the laser pulse was determined by a single exponential fit function, reported previously by Küllig *et al* [26]. As a result, the time constant is nearly constant at a fixed total gas pressure. For example, the time constant amounts to about 1 μs for 5 Pa. Surprisingly, the coil voltage and the coil current change about 2% after the laser pulse (depending on the discharge mode). For both modes, the time constant for the coil voltage relaxation is one order of magnitude higher compared to the time constant for the electron density relaxation. In the E-mode, the coil voltage increases and has its maximum at 5 μs after the laser pulse, whereas the coil voltage in the H-mode decreases to a minimum 10 μs after the laser pulse. Nevertheless, the influence of coil voltage and current variation is not measurable for the electron density, which stays constant during the extrema of both these parameters. However, this effect is not well understood and has to be further investigated.

To analyze the evolution of the negative atomic ion density during the discharge pulse, the onset of the laser shot was varied. The electron and negative atomic ion densities, as well as the electronegativity, are presented over time in relation to the discharge period time in figure 6. The RF power is switched ON at 0% and stays constant for $T_P = 50$ ms. After this time, the RF power is switched OFF at 100%. The electron density raises and reaches its steady state value after about 2.5 ms and 5% of the discharge pulse. It stays approximately constant during the main part of the discharge pulse for about 45 ms. After switching OFF the RF power, the electron density shows the same behavior, with an additional peak in the early afterglow, see section 3.1. The negative atomic ion density also increases in the start-up phase but has a maximum at 1.25 ms and 2.5% of the discharge. After about 10 ms and

Table 1. Elementary collision processes of the negative atomic ion and their corresponding rate coefficients.

#	Reaction	Rate coefficient / $m^3\ s^{-1}$	Reference
1	$e + O_2(X^3\Sigma_g^-) \longrightarrow e + O^+ + O^-$	$k_1 = 7.1 \times 10^{-17}\, T_e^{1/2} \exp(-17/T_e)$	[34]
2	$e + O_2(X^3\Sigma_g^-) \longrightarrow O(^3P) + O^-$	$k_2 = 8.8 \times 10^{-17} \exp(-4.4/T_e)$	[35]
3	$e + O_2(a^1\Delta_g) \longrightarrow O(^3P) + O^-$	$k_3 = 2.28 \times 10^{-16} \exp(-2.29/T_e)$	[36]
4	$e + O_3 \longrightarrow O_2(X^3\Sigma_g^-) + O^-$	$k_4 = 9.3 \times 10^{-16} T_e^{0.62}$	[37]
5	$O_2^- + O(^3P) \longrightarrow O_2(X^3\Sigma_g^-) + O^-$	$k_5 = 3.31 \times 10^{-16}\, (300/T_g)^{1/2}$	[35]
6	$O^- + O_2(a^1\Delta_g) \longrightarrow O(^3P) + O_2^-$	$k_6 = 1.1 \times 10^{-17}\, (300/T_g)^{1/2}$	[38]
7	$O^- + O_3 \longrightarrow O_3^- + O(^3P)$	$k_7 = 5.3 \times 10^{-16}\, (300/T_g)^{1/2}$	[35]
8	$O^- + e \longrightarrow O(^3P) + 2e$	$k_8 = 1.1 \times 10^{-13} \exp(-3.58/T_e)$	[39]
9	$O^- + O(^3P) \longrightarrow O_2(X^3\Sigma_g^-) + e$	$k_9 = 3.0 \times 10^{-16}\, (300/T_g)^{1/2}$	[34]
10	$O^- + O_2(X^3\Sigma_g^-) \longrightarrow O_3 + e$	$k_{10} = 5.0 \times 10^{-21}\, (300/T_g)^{1/2}$	[40]
11	$O^- + O_2(a^1\Delta_g) \longrightarrow O_3 + e$	$k_{11} = 2.2 \times 10^{-17}\, (300/T_g)^{1/2}$	[38]
12	$O^- + O^+ \longrightarrow O(^3P) + O(^3P)$	$k_{12} = 2.7 \times 10^{-13}\, (300/T_g)^{1/2}$	[35]
13	$O^- + O^+ \longrightarrow O(^3P) + O(^1D)$	$k_{13} = 4.9 \times 10^{-16}\, (300/T_g)^{1/2}$	[41]
14	$O^- + O_2^+ \longrightarrow O(^3P) + O_2(X^3\Sigma_g^-)$	$k_{14} = 1.5 \times 10^{-13}\, (300/T_g)^{1/2}$	[42]

20% of the discharge period time, the negative atomic ion density is constant and the discharge is in steady state operation. Consequently, the electronegativity exhibits also a peak at 1.25 ms and reaches a constant value after 10 ms. After 10 ms, the elementary and transport (diffusion) processes are balanced. Finally, the negative atomic ion density quickly decreases in the afterglow within 0.1 ms.

3.3. Rate equation calculation

The negative atomic ion density was calculated using the negative ion rate equation for the steady state. Therefore, a set of 14 elementary collision processes including sources and sinks (ionization, attachment, detachment, charge transfer, recombination) for the negative atomic ions was considered and is listed together with the rate coefficients in table 1. The considered neutral species are ozone O_3, the molecular ground state $O_2(X^3\Sigma_g^-)$, the singlet molecular metastable state $O_2(a^1\Delta_g)$ and the atomic ground state $O(^3P)$. Furthermore, the charged particles are electrons e, the negative O^-, O_2^- and the positive O^+, O_2^+ ions. Consequently, the rate equation for the atomic negative ion is

$$\begin{aligned}\frac{d}{dt}n_{O^-} = &+ (k_1 + k_2)\cdot n_e \cdot n_X + k_3 \cdot n_e \cdot n_a + k_4 \cdot n_e \cdot n_{O_3} \\ &+ k_5 \cdot n_{O_2^-} \cdot n_O - k_6 \cdot n_{O^-} \cdot n_a - k_7 \cdot n_{O^-} \cdot n_{O_3} \\ &- k_8 \cdot n_{O^-} \cdot n_e - k_9 \cdot n_{O^-} \cdot n_O - k_{10} \cdot n_{O^-} \cdot n_X \\ &- k_{11} \cdot n_{O^-} \cdot n_a - (k_{12} + k_{13}) \cdot n_{O^-} \cdot n_{O^+} \\ &- k_{14} \cdot n_{O^-} \cdot n_{O_2^+},\end{aligned} \tag{4}$$

where n_{O^-}, n_e, n_X, n_a, n_{O_3}, $n_{O_2^-}$, n_O, n_{O^+} and $n_{O_2^+}$ are the densities of O^-, e, $O_2(X^3\Sigma_g^-)$, $O_2(a^1\Delta_g)$, O_3, O_2^-, $O(^3P)$, O^+ and O_2^+ respectively. Furthermore, k_i with $i = 1 \ldots 14$ are the rate coefficients to the elementary collision process i listed in table 1.

The amount of the atomic positive ion O^+ was set to 10% in relation to the molecular positive ion O_2^+ [24]. It is furthermore assumed that the amount of the molecular negative ion O_2^- is also 10% in relation to the atomic negative ion O^-, which is well known from the literature [14, 24]. Another assumption is the condition of quasineutrality to determine the atomic positive ion density. The equation (4) is solved for a steady state condition $dn_{O^-}/dt = 0$. Furthermore, the ozone density was set to a constant value of $n_{O_3} = 10^{17}\ m^{-3}$ [17]. The atomic density in the ground state was taken from the global model of Corr *et al* [18] for the considered pressures and electron densities. These values are comparable to other works [17, 20]. The densities of n_e, n_X and n_a as well as the gas (T_g) and electron (T_e) temperature were taken from Wegner *et al* [21]. Together with the assumptions and the input parameters, the equation (4) can be simplified to a quadratic equation. Hence, the density of the negative atomic ions and the electronegativity were determined and are presented in figure 7. The results from the rate equation calculation are qualitatively and quantitatively comparable to the results from the early afterglow and the laser photodetachment. However, the influence of the electron temperature, see Wegner *et al* [21], is seen obviously in the negative atomic density. This influence increases with raising total gas pressure. In particular for 15 Pa, the influence of the electron temperature results in a higher electronegativity compared to the other methods mentioned above. To analyze the main elementary processes for the production and loss of the negative atomic ions, the reaction rates R were determined using the product of the rate coefficient k_i and the involved particle densities of reaction i. The reaction rates for the production (a) and loss (b) of the negative atomic ions are exemplarily shown in figure 8 for a total gas pressure of 5 Pa. The reaction rates allow an estimation of the most important elementary processes. The dissociative electron attachment to the molecular ground state (reaction 2) is the most important source for the negative atomic ion for all operation modes. This is supported by other works [14, 17]. In the E-mode, the ion pair production of the molecular ground state (reaction 1) is also important for the production of O^-. Nevertheless, its influence decreases during the transition from the E- to the E/H-mode and becomes irrelevant compared to other reaction rates. The second important influence for the production of the negative atomic ions in the hybrid as well as in the H-mode

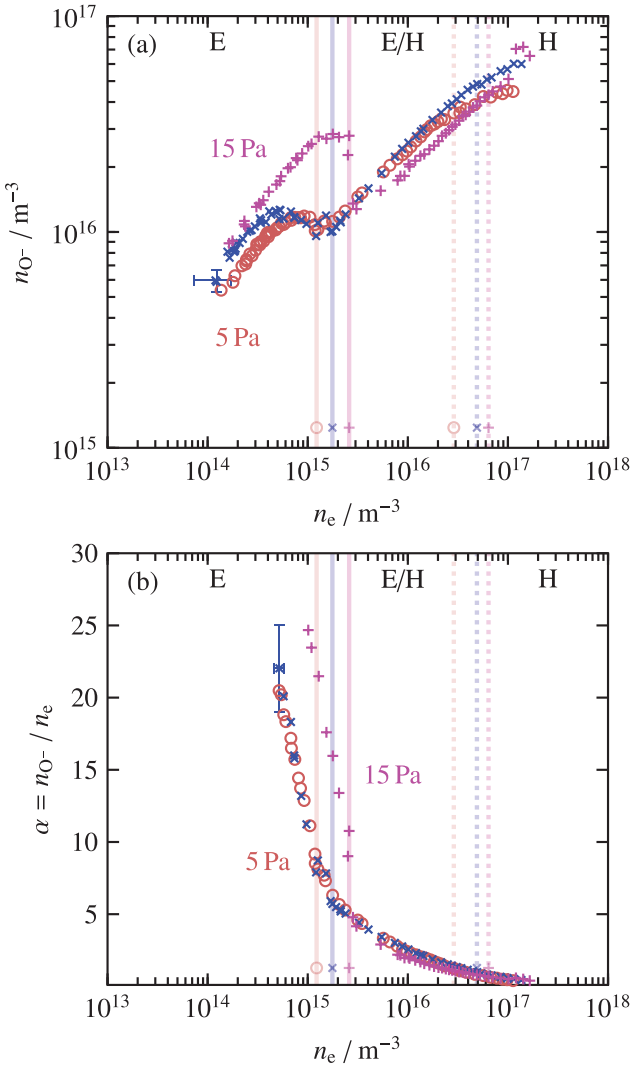

Figure 7. Negative atomic ion density n_{O^-} (a) and electronegativity α (b) determined from rate equation calculation over the electron density n_e for different total gas pressures (5 Pa (∘), 10 Pa (×) and 15 Pa (+)) for the E-mode (E), the hybrid mode (E/H) and for the H-mode (H). The semi-transparent lines with the associated symbols indicate the electron density at which the E-E/H (solid) and the E/H-H (dotted) transition take place.

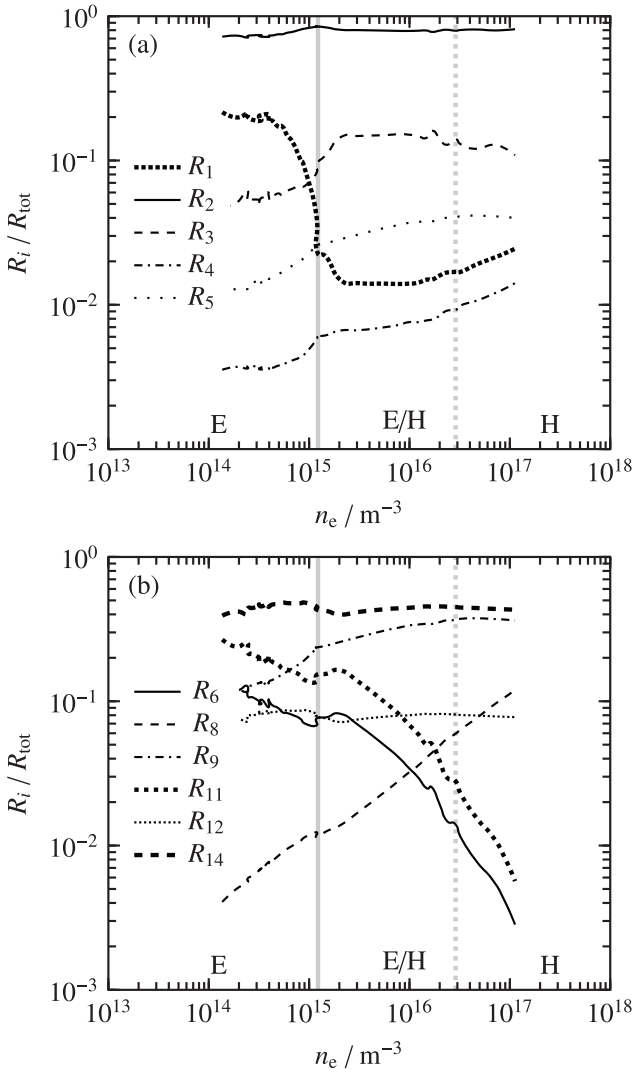

Figure 8. Normalized main reaction rates R_i for the production (a) and loss process (b) of negative ions over the electron density n_e for a total gas pressure of 5 Pa for the E-mode (E), the hybrid mode (E/H) and for the H-mode (H). The semi-transparent lines with the associated symbols indicate the electron density at which the E-E/H (solid) and the E/H-H (dotted) transition take place.

is given by the dissociative attachment reaction with the singlet molecular metastables (reaction 3) although the density of metastables decreases in these modes [21]. The loss of the negative atomic ions is mainly determined by the recombination with the positive molecular ion (rate 14) and the detachment with the atomic ground state (reaction 9). This is also in good agreement with previous papers [14, 16–19] but contrary to the study of Toneli *et al* [20], which explained the small contribution of $O_2(a^1\Delta_g)$ compared to $O_2(b^1\Sigma_g^+)$ which is not included in this work. Here, the detachment with the singlet molecular metastables (reaction 6 and 11) is mainly important in the E-mode and also leads to the electron release in the early afterglow [43]. The ion–ion recombination with the positive atomic ion (reaction 12) and the detachment with electrons (reaction 8) become important in the E/H- and H-mode. The charge transfer with ozone (reaction 7) and the detachment with the molecular ground state (reaction 10) can be neglected for the loss of the negative atomic ions.

All methods mentioned above reveal comparable results for the negative atomic ion density and furthermore the electronegativity. For the comparison of these methods (electron density peak in the early after glow EDP, laser photodetachment LPD and rate equation calculation REC), the electronegativity is exemplarily shown in figure 9 for a total gas pressure of 5 Pa. The experimental investigations, as well as the rate equation calculation, yield comparable results regarding the negative atomic ion density and electronegativity. Summarizing, the discharge is strongly electronegative in the E-mode, with an electronegativity of about 25. During the E-E/H transition, the electronegativity decreases to about 5 at the transition point between the E- and E/H-mode. The electronegativity decreases further in the E/H- and H-mode and reaches a value of about 0.5 at the E/H-H transition. The shrinking electronegativity is the result of the increasing dissociation of the

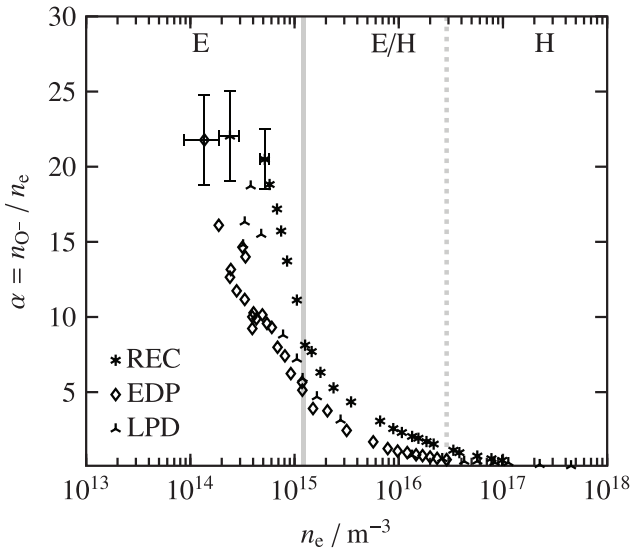

Figure 9. Electronegativity α determined from the electron density peak in the early afterglow (◊ EDP), laser photodetachment (⅄ LPD) and rate equation calculation (∗ REC) over the electron density n_e for a total gas pressure of 5 Pa for the E-mode (E), the hybrid mode (E/H) and for the H-mode (H). The semi-transparent lines with the associated symbols indicate the electron density at which the E-E/H (solid) and the E/H-H (dotted) transition take place.

molecular ground state, which is important for the production of negative atomic ions [18]. Furthermore, the increasing dissociation during the E-H transition leads to a higher atomic ground state density which is an important partner for the loss process of the negative atomic ion. The negative atomic ion density is in good agreement with the work of Corr *et al* [18]. In the E-mode, the electronegativity is higher by a factor of 2 compared to those reported by Corr *et al* [18]. However, the electronegativity in the H-mode is comparable to the literature [16, 18, 19]. The electronegativity measured here is much higher compared to a CCP of a similar experiment [26], but the trend with increasing RF power is comparable to results previously published [14, 16, 18, 19].

4. Conclusion and summary

This paper presents and discusses results regarding the negative atomic ion density and furthermore the electronegativity of an inductively coupled RF oxygen discharge. In particular, the mode transition and its influence on the electronegativity were investigated using comprehensive plasma diagnostics and a rate equation calculation. The negative atomic ion density was experimentally determined from the electron density peak in the early afterglow, which is due to collisional detachment of atomic negative ions with singlet molecular metastables. Furthermore, Gaussian beam microwave interferometry combined with laser photodetachment provide the complete behavior of the electronegativity during the E-H transition. Additionally, temporally resolved measurements of the negative atomic ion density in pulsed mode operation of the ICP show that a steady state is reached after 10 ms. The rate equation calculation also provides the electronegativity and gives information about the most important elementary collision processes. All methods apply nearly the same behavior of the electronegativity during the mode transition. The negative atomic ion density in the E-mode is greater by a factor of about 25 compared to the electron density, and exhibits a strong electronegativity. During the transition from the E- to the H-mode, the discharge becomes more electropositive and reaches an electronegativity of about 0.5 at the E/H-H transition and 0.1 in the H-mode. The most important elementary collision process for the production of the negative atomic ions is the dissociative electron attachment to the molecular ground state. The ion–ion recombination of negative atomic ions with the positive molecular ions and the detachment with the atomic ground state contribute significantly to the loss process of the negative atomic ions.

Together with the investigations which are presented in the first part [21] of this series of two papers and the results presented here, a whole set of plasma parameters is implemented. These results can be used for 3D modeling and simulation of the E-H transition which may contribute to more knowledge about the physical processes of this mode transition.

Acknowledgments

This work was supported by the Deutsche Forschungsgemeinschaft (DFG) in the framework of the Sonderforschungsbereich Transregio 24 ‘Fundamentals of Complex Plasmas’, project B5.

References

[1] Keller J H 1996 *Plasma Sources Sci. Technol.* **5** 166
[2] Im Y H, Park J S, Choi C S, Choi R J, Hahn Y B, Lee S-H and Lee J-K 2001 *J. Vac. Sci. Technol.* A **19** 1315
[3] Shin M H, Park M S, Lee N-E, Kim J, Kim C Y and Ahn J 2006 *J. Vac. Sci. Technol.* A **24** 1373
[4] Carlström C F, van der Heijden R, Karouta F, van der Heijden R W, Salemink H W M and van der Drift E 2006 *J. Vac. Sci. Technol.* B **24** L6
[5] Ono T, Akagi T and Ichiki T 2009 *J. Appl. Phys.* **105** 013314
[6] von Keudell A *et al* 2010 *Plasma Process. Polym.* **7** 327
[7] Kylián O, Denis B, Stapelmann K, Ruiz A, Rauscher H and Rossi F 2011 *Plasma Process. Polym.* **8** 1137
[8] Douglas E A, Stevens J, Fishgrab K, Ford C, Shul R J and Pearton S J 2012 *J. Vac. Sci. Technol.* B **30** 06FF06
[9] Yoshino K, Matsumoto H, Iwasaki T, Kinoshita S, Noda K and Iwamori S 2013 *Vacuum* **93** 84
[10] Nighan W L and Wiegand W J 1974 *Phys. Rev.* A **10** 922
[11] Lieberman M A, Lichtenberg A J and Marakhtanov A M 1999 *Appl. Phys. Lett.* **75** 3617
[12] Corr C S, Steen P G and Graham W G 2003 *Plasma Sources Sci. Technol.* **12** 265
[13] Küllig C, Wegner Th and Meichsner J 2015 *Phys. Plasmas* **22** 043515
[14] Stoffels E, Stoffels W W, Vender D, Kando M, Kroesen G M W and de Hoog F J 1995 *Phys. Rev.* E **51** 2425
[15] Katsch H M, Sturm T, Quandt E and Döbele H F 2000 *Plasma Sources Sci. Technol.* **9** 323
[16] Katsch H M, Manthey C and Döbele H F 2003 *Plasma Sources Sci. Technol.* **12** 475
[17] Gudmundsson J T, Kouznetsov I G, Patel K K and Lieberman M A 2001 *J. Phys. D: Appl. Phys.* **34** 1100
[18] Corr C S, Gomez S and Graham W G 2012 *Plasma Sources Sci. Technol.* **21** 055024

[19] Gudmundsson J T 2004 *J. Phys. D: Appl. Phys.* **37** 2073
[20] Toneli D A, Pessoa R S, Roberto M and Gudmundsson J T 2015 *J. Phys. D: Appl. Phys.* **48** 325202
[21] Wegner Th, Küllig C and Meichsner J 2017 On the E-H transition in inductively coupled radio frequency oxygen discharges: I. Density and temperature of electrons, ground state and singlet metastable molecular oxygen *Plasma Sources Sci. Technol.* **26** 025006
[22] Wegner Th, Küllig C and Meichsner J 2015 *Contrib. Plasma Phys.* **55** 728
[23] Dittmann K, Küllig C and Meichsner J 2012 *Plasma Sources Sci. Technol.* **21** 024001
[24] Vender D, Stoffels W W, Stoffels E, Kroesen G M W and de Hoog F J 1995 *Phys. Rev.* E **51** 2436
[25] Küllig C, Dittmann K, Wegner Th, Sheykin I, Matyash K, Loffhagen D, Schneider R and Meichsner J 2012 *Contrib. Plasma Phys.* **52** 836
[26] Küllig C, Dittmann K and Meichsner J 2010 *Plasma Sources Sci. Technol.* **19** 065011
[27] Goldsmith P F 1998 *Quasioptical Systems* (Piscataway, NJ: IEEE Press)
[28] Schiffer C and Uhlenbusch J 1995 *Plasma Sources Sci. Technol.* **4** 345
[29] Burch D S, Smith S J and Branscomb L M 1958 *Phys. Rev.* **112** 171
[30] Schulze J, Donkó Z, Heil B G, Luggenhölscher D, Mussenbrock T, Brinkmann R P and Czarnetzki U 2008 *J. Phys. D: Appl. Phys.* **41** 105214
[31] Wegner Th, Küllig C and Meichsner J 2014 *IEEE Trans. Plasma Sci.* **42** 2830
[32] Wegner Th, Küllig C and Meichsner J 2015 *Plasma Sources Sci. Technol.* **24** 044001
[33] Schulze J, Derzsi A, Dittmann K, Hemke T, Meichsner J and Donkó Z 2011 *Phys. Rev. Lett.* **107** 275001
[34] Lieberman A M 2005 *Principles of Plasma Discharges and Materials Processing* (New York: Wiley)
[35] Eliasson B and Kogelschatz U 1986 *Basic Data for Modelling of Electrical Discharges in Gases: Oxygen* (*Brown Boveri Forschungszentrum CH-5405 Baden*) (Baden: ABB Asea Brown Boveri)
[36] Gudmundsson J T, Marakhtanov A M, Patel K K, Gopinath V P and Lieberman M A 2000 *J. Phys. D: Appl. Phys.* **33** 1323
[37] Senn G, Skalny J D, Stamatovic A, Mason N J, Scheier P and Märk T D 1999 *Phys. Rev. Lett.* **82** 5028
[38] Upschulte B L, Marinelli W J and Green B D 1994 *J. Phys. Chem.* **98** 837
[39] Vejby-Christensen L, Kella D, Mathur D, Pedersen H B, Schmidt H T and Andersen L H 1996 *Phys. Rev.* A **53** 2371
[40] Kossyi I A, Kostinsky A Y, Matveyev A A and Silakov V P 1992 *Plasma Sources Sci. Technol.* **1** 207
[41] Hayashi D and Kadota K 1998 *J. Appl. Phys.* **83** 697
[42] Lieberman M A, Lee C, Graves D B and Hess D W 1994 *J. Electrochem. Soc.* **141** 1546
[43] Küllig C, Dittmann K and Meichsner J 2012 *Phys. Plasmas* **19** 073517
[44] Brockhaus A, Leu G F, Selenin V, Tarnev K and Engemann J 2006 *Plasma Sources Sci. Technol.* **15** 171